

Ultra-high thermal conductivity in hexagonal BC₆N- An efficient material for nanoscale thermal management- A first principles study

Rajmohan Muthaiah, Jivtesh Garg

School of Aerospace and Mechanical Engineering, University of Oklahoma, Norman,
OK-73019, USA

Abstract: Engineering materials with high thermal conductivity are of fundamental interest for efficiently dissipating heat in micro/nanoelectronics. Using first principles computations we report an ultra-high thermal conductivity of 2090 Wm⁻¹K⁻¹ (1395 Wm⁻¹K⁻¹) for hexagonal pure (natural) BC₆N(*h*-BC₆N). This value is among the highest thermal conductivities known after diamond and cubic boron arsenide. This ultra-high lattice thermal conductivity (*k*) is mainly attributed with high phonon group velocities of both acoustic and optical phonons arising from strong C-C and B-N bonds as well as the light atomic mass of the constituent elements such as boron (B), carbon (C) and nitrogen (N). We also report size dependent thermal conductivity of *h*-BC₆N nanostructures by including boundary scattering. At room temperature (300 K) and at nanoscale length (*L*) of 100 nm, a high *k* value of 175 Wm⁻¹K⁻¹ is observed (higher than the bulk *k* value of silicon). Optical phonons with large group velocities are mainly responsible for this high thermal conductivity in *h*-BC₆N nanostructures. High thermal conductivity of *h*-BC₆N makes it a candidate material for heat dissipation in micro/nano thermal management applications.

Keywords: BC₆N, nanoelectronics, ultra-high thermal conductivity, first principles calculations

Introduction: Continued decrease in transistor length has led to the issue of hot spots¹ in electronic chips. Heat removal in micro/nanoelectronics is a fundamental issue that limits its performance and reliability^{2, 3}. High thermal conductivity materials can play a strong role in improving heat dissipation. Cubic⁴⁻⁶ and hexagonal diamond⁷ (also known as lonsdaleite) has been reported as the most thermally conductive materials on earth due to the strong covalent bonds and light atomic mass of carbon atoms. Likewise, boron⁸⁻¹⁶ based compounds were reported with high thermal conductivity in bulk and nanostructured materials due to high phonon group velocity arising from the light atomic mass. Recently, Sadeghi *et al.*, reported a high thermal conductivity of 2073 Wm⁻¹K⁻¹ for the hexagonal BC₂N(*h*-BC₂N)⁸ with optical phonons has considerable phonon group velocities which are beneficial for the thermal transport in nanostructures. Likewise, Shafique *et al.*, reported a high thermal conductivity of 1275 Wm⁻¹K⁻¹ for the monolayer graphene like

BC₂N¹². Mortazavi *et al.*, reported an ultra-high thermal conductivity 1710 Wm⁻¹K⁻¹ for the monolayer BC₆N¹⁷ but its counterpart of bulk thermal conductivity is yet to be reported. In this work, we analyzed the thermal conductivity of bulk and nanostructured hexagonal BC₆N(*h*-BC₆N) through first principles calculations. Our first principles calculations reveal an ultra-high bulk thermal conductivity (*k*) of 2090 Wm⁻¹K⁻¹(1395 Wm⁻¹K⁻¹) for the pure (natural) hexagonal BC₆N which is among the highest thermal conductivity values ever reported (lower only to diamond and boron arsenide¹³). Likewise, at nanometer length scales such as 100 nm, computed room temperature thermal conductivity of 175 Wm⁻¹K⁻¹, indicating *h*-BC₆N will be a candidate material for thermal management in nanoelectronics. We systematically investigated the elastic constants, mode-contribution thermal conductivity of transverse acoustic (TA), longitudinal acoustic (LA) and optical phonon modes, phonon group velocity, phonon scattering rates and phonon mean free paths. We noticed that, optical phonons with considerable phonon group velocities and phonon lifetimes, contribute significantly to overall thermal conductivity in *h*-BC₆N.

Computational methods: First principles computations were performed using local density approximations¹⁸ with norm-conserving pseudopotentials within QUANTUM ESPRESSO¹⁹ package. The geometry of the hexagonal BC₆N(*h*-BC₆N) with 8 atoms unit cell is optimized until the forces on all atoms are less than 10⁻⁵ eV Å⁻¹ and the energy difference is converged to 10⁻¹⁵ Ry. A plane-wave cutoff energy of 80 Ry was used. Electronic calculations were performed using 12 x 12 x 4 Monkhorst-Pack²⁰ *k*-point mesh. Optimized *h*-BC₆N structure with lattice constants of a=2.4802 Å and c/a=3.3438 is shown in Fig. 1. Elastic constants were computed using QUANTUM ESPRESSO thermo_pw package and Voigt-Reuss-Hill approximation²¹ is used to calculate the bulk modulus(B), Young's Modulus(E) and shear modulus(G). Dynamical matrix and harmonic force constants were computed using 12 x 12 x 4 q-grid. 6 x 6 x 2 q-points were

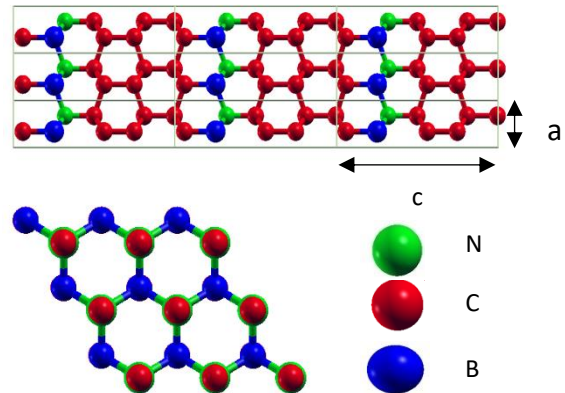


Figure 1: *h*-BC₆N crystal structure with lattice parameters a= 2.4802 Å and c/a=3.3438. Blue, red and green represents the boron, carbon and nitrogen atoms respectively.

used to compute the anharmonic force constants using QUANTUM ESPRESSO D3Q²²⁻²⁴ package. Acoustic sum rules were imposed on both harmonic and anharmonic interatomic force constants. Lattice thermal conductivity(k) is calculated by solving phonon Boltzmann transport equation (PBTE)^{22, 24, 25}. Thermal conductivity (k) in the single mode relaxation time (SMRT) approximation²⁶ (usually the first approximation in solution of PBTE) is given by,

$$k_{\alpha} = \frac{\hbar^2}{N\Omega k_b T^2} \sum_{\lambda} v_{\alpha\lambda}^2 \omega_{\lambda}^2 \bar{n}_{\lambda} (\bar{n}_{\lambda} + 1) \tau_{\lambda} \quad (1)$$

where, α , \hbar , N , Ω , k_b , T , are the cartesian direction, Planck constant, size of the q mesh, unit cell volume, Boltzmann constant, and absolute temperature respectively. λ represents the vibrational mode (\mathbf{qj}) (\mathbf{q} is the wave vector and j represent phonon polarization). ω_{λ} , \bar{n}_{λ} , and $v_{\alpha\lambda}$ ($= \partial\omega_{\lambda}/\partial q$) are the phonon frequency, equilibrium Bose-Einstein population and group velocity along cartesian direction α , respectively of a phonon mode λ . ω_{λ} , \bar{n}_{λ} , and $c_{\alpha\lambda}$ are derived from the knowledge of phonon dispersion computed using 2nd order IFCs. τ_{λ} is the phonon lifetime and is computed using the following equation,

$$\frac{1}{\tau_{\lambda}} = \pi \sum_{\lambda'\lambda''} |V_3(-\lambda, \lambda', \lambda'')|^2 \times [2(n_{\lambda'} - n_{\lambda''})\delta(\omega(\lambda) + \omega(\lambda') - \omega(\lambda'')) + (1 + n_{\lambda'} + n_{\lambda''})\delta(\omega(\lambda) - \omega(\lambda') - \omega(\lambda''))] \quad (2)$$

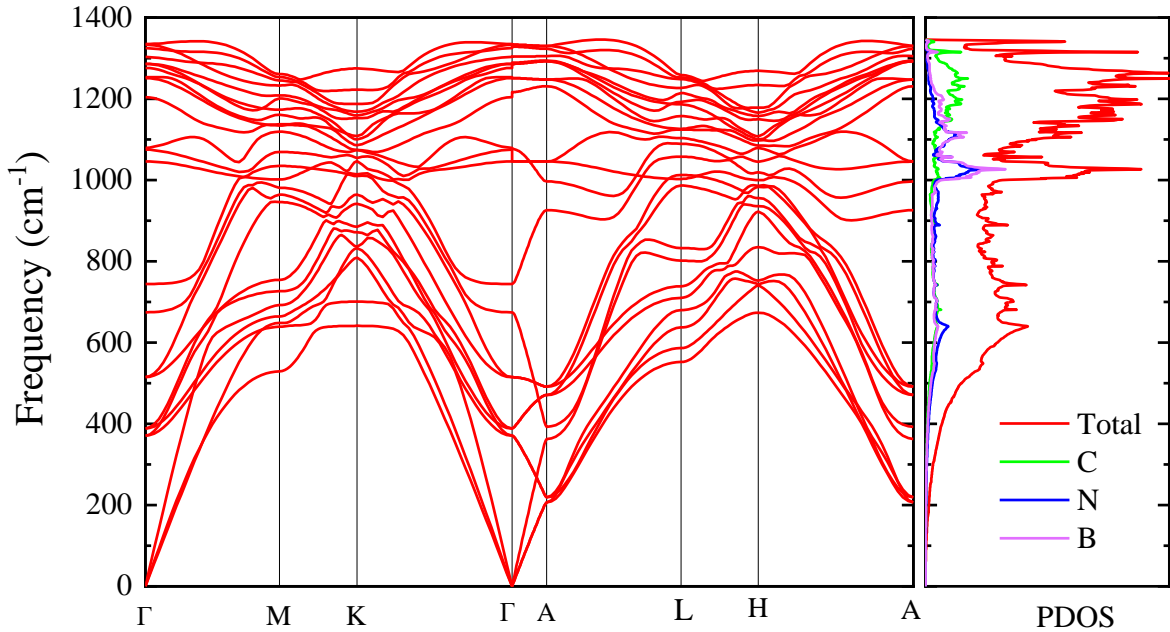


Figure 2: Phonon dispersion and phonon density of states for the hexagonal BC₆N with lattice constants $a= 2.4802 \text{ \AA}$ and $c/a=3.3438$. Green, blue and purple color represents the contributions from carbon (C), nitrogen (N) and boron (B) respectively.

where, $\frac{1}{\tau_\lambda}$ is the anharmonic scattering rate due to phonon-phonon interactions and $V_3(-\lambda, \lambda', \lambda'')$ are the three-phonon coupling matrix elements computed using both harmonic and anharmonic interatomic force constants. Phonon linewidth and lattice thermal conductivity were calculated iteratively using QUANTUM ESPRESSO thermal2 code with 30 x 30 x 10 q -mesh and 0.05 cm⁻¹ smearing until the Δk values are converged to 1.0e⁻⁵ Wm⁻¹K⁻¹. Iterative results were converged after 6 iterations. Casimir scattering²⁷ is imposed for size dependence thermal conductivity calculations for the nanostructured *h*-BC₆N.

Results and Discussion:

Phonon dispersion and phonon density of states for the hexagonal BC₆N with its equilibrium lattice constants $a = 2.4802 \text{ \AA}$ and $c/a = 3.3438$ is shown in Fig 2. Positive phonons frequencies of all the phonon branches indicate the dynamical stability of *h*-BC₆N. To validate the mechanical stability of the system, we calculated elastic constants to check the Born stability criteria²⁸. Elastic constants of *h*-BC₆N are listed in Table 1 and compared against *h*-diamond and *h*-BC₂N. The calculated elastic constants satisfied the Born stability criteria of $C_{66} = (C_{11} - C_{12})/2$, $C_{11} > C_{12}$, $C_{33}(C_{11} + C_{12}) > 2(C_{13})$, $C_{44} > 0$, $C_{66} > 0$, and hence the system is mechanically stable. Bulk modulus(B), Young modulus(E) and Shear modulus(G) based on Voigt-Reuss-Hill approximation are also listed in Table 1. The computed values are slightly lower than the hexagonal diamond. These elastic constants and positive frequencies in phonon dispersion indicate the mechanical and dynamical stability of *h*-BC₆N.

Table 1: Elastic constants (in GPa) of *h*-BC₆N, *h*-Diamond and *h*-BC₂N.

Material	C11	C33	C44	C66	C12	C13	Bulk Modulus(B)	Young modulus(E)	Shear Modulus(G)
<i>h</i> -BC ₆ N	1182.98	1298.11	438.90	537.20	108.58	20.33	440.00	1107.40	512.30
<i>h</i> -Diamond	1251.52	1367.74	483.00	579.40	92.61	20.00	450.74	1182.45	556.31
<i>h</i> -BC ₂ N	1091.10	1146.23	399.50	498.70	93.60	2.97	391.90	1007.40	470.05

Temperature dependence lattice thermal conductivity(k) of the pure (solid lines) and naturally (dotted lines) occurring *h*-BC₆N, obtained by solving the phonon Boltzmann transport equation exactly, is shown along a-axis and c-axis in Fig 3a. At 300 K, thermal conductivity of pure and

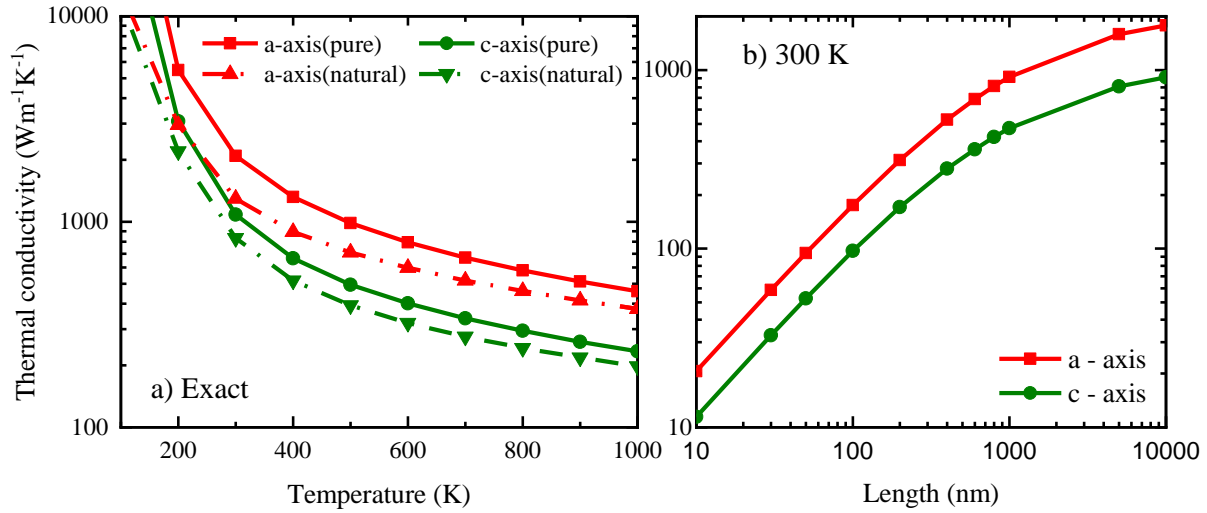


Figure 3a): Temperature dependent lattice thermal conductivity along a and c axis for pure and naturally occurring $h\text{-BC}_6\text{N}$. b) Room temperature size dependence thermal conductivity of pure $h\text{-BC}_6\text{N}$.

naturally occurring $h\text{-BC}_6\text{N}$ is $2090 \text{ Wm}^{-1}\text{K}^{-1}$ ($1082 \text{ Wm}^{-1}\text{K}^{-1}$) and $1395 \text{ Wm}^{-1}\text{K}^{-1}$ ($832 \text{ Wm}^{-1}\text{K}^{-1}$) respectively along the a-axis (c-axis). k of naturally occurring $h\text{-BC}_6\text{N}$ is 33.25% lower than the pure $h\text{-BC}_6\text{N}$. Thermal conductivity for naturally occurring $h\text{-BC}_6\text{N}$ was computed by introducing phonon scattering arising out of mass-disorder due to random distribution of isotopes of Boron, Carbon and Nitrogen throughout the crystal. The small mass variation in isotopes of B (atomic mass of 10.012 a.u with 19.9% concentration and atomic mass of 11.009 a.u with 80.1% concentration), C (atomic mass of 12 a.u with 98.93% concentration and 13.0033 a.u with 1.07% concentration) and N (atomic mass of 14.003 a.u with 99.636% concentration and 15.0 a.u with 1.07% concentration) atoms²⁹, induces moderate additional phonon scattering, causing only 33.25%

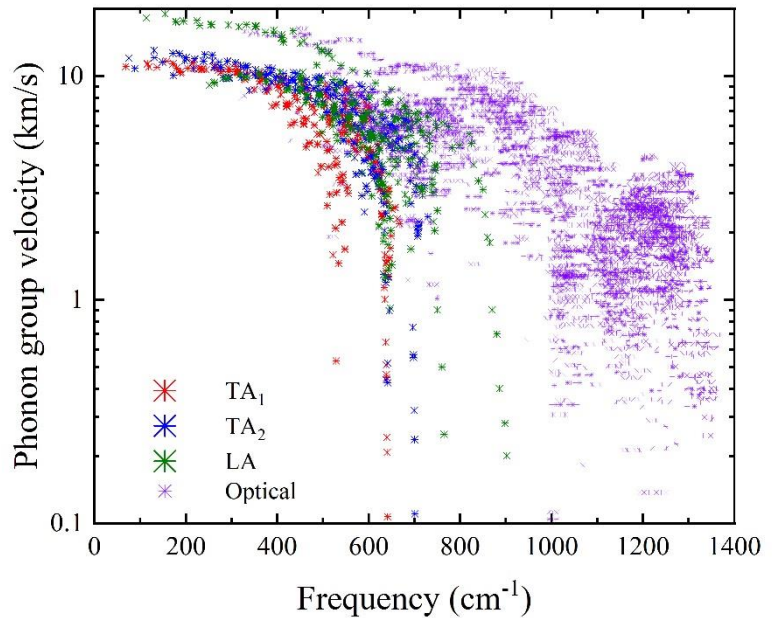


Figure 4: Phonon group velocity of TA₁, TA₂, LA and Optical phonon modes of $h\text{-BC}_6\text{N}$.

decrease in thermal conductivity of naturally occurring h -BC₆N relative to the pure case. Lattice thermal conductivity using single mode relaxation approximation (SMA) is shown in supplementary Fig S1. At 300K, lattice thermal conductivity of h -BC₆N within the SMA is 1601 Wm⁻¹K⁻¹ (999 Wm⁻¹K⁻¹) along the a-axis (c-axis); this value is 23.3% (7.67%) lower than the iterative solution.

This ultra-high thermal conductivity of h -BC₆N is mainly attributed to high phonon frequencies (ω_λ) and phonon group velocities ($= \partial\omega_\lambda/\partial q$) of both acoustic and optical phonons. These high frequencies are due to the strong C-C, B-C and B-N bonds and the light atomic mass of the constituent atoms B, C and N. These strong bonds are verified by the elastic constants presented in Table 1 with diamond and h -BC₂N. Bulk modulus and Young modulus for h -BC₆N is close to that of diamond. This is due to the strong covalent bond network through sp^3 hybridization of the atoms.

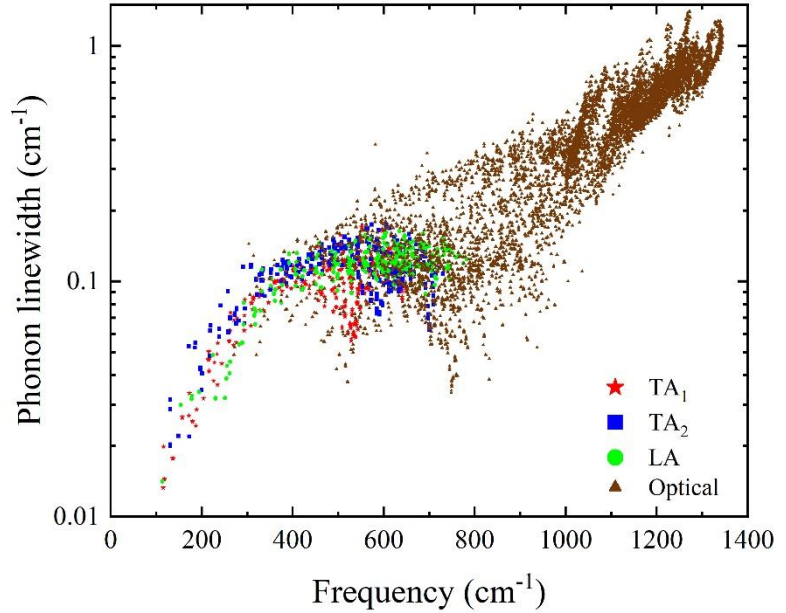


Figure 5: Phonon linewidths of TA₁, TA₂, LA and optical phonons for h -BC₆N. Red, Blue, Green and brown color represents the TA₁, TA₂, LA and optical phonons respectively.

To elucidate further, we analyzed the mode contribution thermal conductivity, phonon group velocities and phonon scattering rates of transverse acoustic (TA), longitudinal acoustic (LA) and optical phonons. At 300 K, we observed that, TA₁, TA₂, LA and optical phonons contribute 21.9% (16.62%), 18.11% (15.77%), 17.37% (18.87%) and 42.62% (48.74%) to overall thermal conductivity, respectively, along a-axis (c-axis). Typically, acoustic phonons are considered as major heat carrier phonons and optical phonons serve as a scattering channels for the acoustic phonons³⁰. It is interesting to note that in BC₆N, optical phonons also contribute significantly to overall thermal conductivity. This is mainly due to the fact that optical phonons have considerable

high phonon group velocities (Fig 4) and phonon lifetimes (inverse of the phonon linewidths as shown in Fig 5).

To explore the thermal transport in nanostructures, we have computed the size dependent thermal conductivity of h -BC₆N by introducing phonon boundary/Casimir²⁷ scattering. We have computed the length dependence of only pure h -BC₆N. Length dependent thermal conductivity(k) of h -BC₆N between 10 nm and 10 μ m is shown in Fig 3b. For an example, at nanometer length scales of $L = 100$ nm, room temperature k of h -BC₆N is $175 \text{ Wm}^{-1}\text{K}^{-1}$ along the a-axis which is significantly higher than the thermal conductivity of bulk silicon³¹. To understand this further, we computed the phonon mean free paths of TA₁, TA₂, LA and optical phonon modes as shown in Fig 6. We can observe that acoustic phonons have mean free path higher than 100 nm and will be scattered significantly for nanostructures smaller than 100 nm, due to boundary scattering. Optical phonon meanfreepaths, however, are in the range of nanometers, contributing to the high nanoscale thermal conductivity in h -BC₆N.

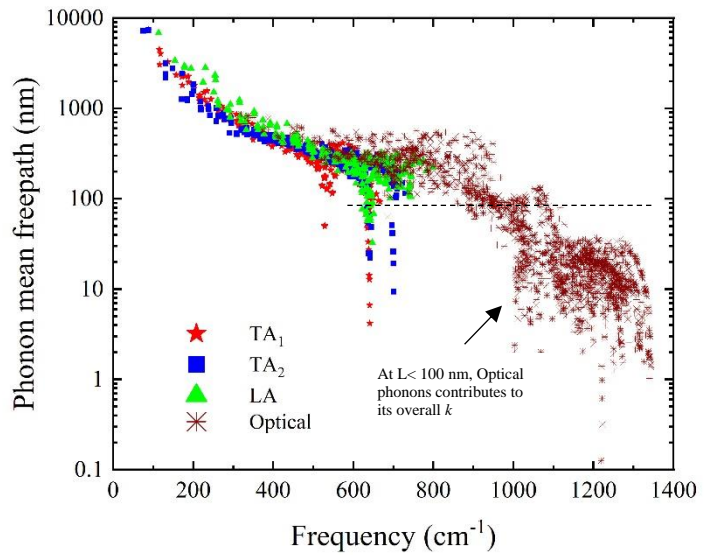


Figure 6: Phonon mean free path of TA₁, TA₂, LA and Optical phonons for h -BC₆N

Conclusion: In this work, by solving Boltzmann transport equation with first principles calculations, we report an ultra-high lattice thermal conductivity of $2090 \text{ Wm}^{-1}\text{K}^{-1}$ ($1082 \text{ Wm}^{-1}\text{K}^{-1}$) along a-axis(c-axis) for pure hexagonal BC₆N(h -BC₆N) which is the 3rd highest reported thermal conductivity after diamond and cubic boron arsenide. This ultra-high thermal conductivity is mainly attributed to high phonon frequencies and phonon group velocities arising from the strong C-C, B-C and B-N bonds and the light atomic mass of the constituent atoms B, C and N. We also observed a significant phonon scattering due to isotopic disorder. Elastic constants show that h -BC₆N is ultrahard with elastic constants almost equal to diamond. We also computed the size

dependent thermal conductivity of *h*-BC₆N between 10 nm and 10000 nm. At nanometer length scales of *L*=100 nm, a high room temperature thermal conductivity of 175 Wm⁻¹K⁻¹ was reported. This points to the promising nature of *h*-BC₆N as candidate for nanoscale thermal management applications.

Conflicts of Interest

There are no conflicts of interest to declare.

Acknowledgements

RM and JG acknowledge support from National Science Foundation CAREER award under Award No. #1847129. We also acknowledge OU Supercomputing Center for Education and Research (OSCER) for providing computing resources for this work.

Data Availability: The raw/processed data required to reproduce these findings can be shared upon request.

References:

1. Ferain, I.; Colinge, C. A.; Colinge, J.-P., Multigate transistors as the future of classical metal–oxide–semiconductor field-effect transistors. *Nature* **2011**, *479* (7373), 310-316.
2. Balandin, A. In *Thermal Management of Nanoelectronics and 3-d Electronics. Thermal Challenges at Nanoscale Graphene as a Thermal Management Material*, 2011.
3. Bar-Cohen, A.; Wang, P.; Rahim, E., Thermal management of high heat flux nanoelectronic chips. *Microgravity Science and Technology* **2007**, *19* (3), 48-52.
4. Wei, L.; Kuo, P. K.; Thomas, R. L.; Anthony, T. R.; Banholzer, W. F., Thermal conductivity of isotopically modified single crystal diamond. *Physical Review Letters* **1993**, *70* (24), 3764-3767.
5. Burgemeister, E., Thermal conductivity of natural diamond between 320 and 450 K. *Physica B+ C* **1978**, *93* (2), 165-179.
6. Broido, D. A.; Lindsay, L.; Ward, A., Thermal conductivity of diamond under extreme pressure: A first-principles study. *Physical Review B* **2012**, *86* (11), 115203.
7. Chakraborty, P.; Xiong, G.; Cao, L.; Wang, Y., Lattice thermal transport in superhard hexagonal diamond and wurtzite boron nitride: A comparative study with cubic diamond and cubic boron nitride. *Carbon* **2018**, *139*, 85-93.
8. Nayeb Sadeghi, S.; Vaez Allaei, S. M.; Zebarjadi, M.; Esfarjani, K., Ultra-high lattice thermal conductivity and the effect of pressure in superhard hexagonal BC₂N. *Journal of Materials Chemistry C* **2020**.

9. Muthaiah, R.; Tarannum, F.; Annam, R. S.; Nayal, A. S.; Danayat, S.; Garg, J., Thermal conductivity of hexagonal BC2P – a first-principles study. *RSC Advances* **2020**, *10* (70), 42628-42632.
10. Muthaiah, R.; Garg, J., Strain tuned high thermal conductivity in boron phosphide at nanometer length scales – a first-principles study. *Physical Chemistry Chemical Physics* **2020**, *22* (36), 20914-20921.
11. Yuan, C.; Li, J.; Lindsay, L.; Cherns, D.; Pomeroy, J. W.; Liu, S.; Edgar, J. H.; Kuball, M., Modulating the thermal conductivity in hexagonal boron nitride via controlled boron isotope concentration. *Communications Physics* **2019**, *2* (1), 43.
12. Shafique, A.; Shin, Y.-H., Ultrahigh and anisotropic thermal transport in the hybridized monolayer (BC2N) of boron nitride and graphene: a first-principles study. *Physical Chemistry Chemical Physics* **2019**, *21* (31), 17306-17313.
13. Lindsay, L.; Broido, D. A.; Reinecke, T. L., First-Principles Determination of Ultrahigh Thermal Conductivity of Boron Arsenide: A Competitor for Diamond? *Physical Review Letters* **2013**, *111* (2), 025901.
14. Lindsay, L.; Broido, D. A.; Reinecke, T. L., Ab initio thermal transport in compound semiconductors. *Physical Review B* **2013**, *87* (16), 165201.
15. Zheng, Q.; Li, S.; Li, C.; Lv, Y.; Liu, X.; Huang, P. Y.; Broido, D. A.; Lv, B.; Cahill, D. G., High Thermal Conductivity in Isotopically Enriched Cubic Boron Phosphide. *Advanced Functional Materials* **2018**, *28* (43), 1805116.
16. Kang, J. S.; Wu, H.; Hu, Y., Thermal Properties and Phonon Spectral Characterization of Synthetic Boron Phosphide for High Thermal Conductivity Applications. *Nano Letters* **2017**, *17* (12), 7507-7514.
17. Mortazavi, B.; Shahrokhi, M.; Raeisi, M.; Zhuang, X.; Pereira, L. F. C.; Rabczuk, T., Outstanding strength, optical characteristics and thermal conductivity of graphene-like BC3 and BC6N semiconductors. *Carbon* **2019**, *149*, 733-742.
18. Ceperley, D. M.; Alder, B. J., Ground State of the Electron Gas by a Stochastic Method. *Physical Review Letters* **1980**, *45* (7), 566-569.
19. Giannozzi, P.; Baroni, S.; Bonini, N.; Calandra, M.; Car, R.; Cavazzoni, C.; Ceresoli, D.; Chiarotti, G. L.; Cococcioni, M.; Dabo, I.; Dal Corso, A.; de Gironcoli, S.; Fabris, S.; Fratesi, G.; Gebauer, R.; Gerstmann, U.; Gougoussis, C.; Kokalj, A.; Lazzeri, M.; Martin-Samos, L.; Marzari, N.; Mauri, F.; Mazzarello, R.; Paolini, S.; Pasquarello, A.; Paulatto, L.; Sbraccia, C.; Scandolo, S.; Sclauzero, G.; Seitsonen, A. P.; Smogunov, A.; Umari, P.; Wentzcovitch, R. M., QUANTUM ESPRESSO: a modular and open-source software project for quantum simulations of materials. *Journal of Physics: Condensed Matter* **2009**, *21* (39), 395502.
20. Monkhorst, H. J.; Pack, J. D., Special points for Brillouin-zone integrations. *Physical Review B* **1976**, *13* (12), 5188-5192.
21. Chung, D. H.; Buessem, W. R., The Voigt-Reuss-Hill (VRH) Approximation and the Elastic Moduli of Polycrystalline ZnO, TiO2 (Rutile), and α -Al2O3. *Journal of Applied Physics* **1968**, *39* (6), 2777-2782.
22. Paulatto, L.; Errea, I.; Calandra, M.; Mauri, F., First-principles calculations of phonon frequencies, lifetimes, and spectral functions from weak to strong anharmonicity: The example of palladium hydrides. *Physical Review B* **2015**, *91* (5), 054304.

23. Paulatto, L.; Mauri, F.; Lazzeri, M., Anharmonic properties from a generalized third-order ab initio approach: Theory and applications to graphite and graphene. *Physical Review B* **2013**, *87* (21), 214303.
24. Fugallo, G.; Lazzeri, M.; Paulatto, L.; Mauri, F., Ab initio variational approach for evaluating lattice thermal conductivity. *Physical Review B* **2013**, *88* (4), 045430.
25. Garg, J.; Bonini, N.; Marzari, N., First-Principles Determination of Phonon Lifetimes, Mean Free Paths, and Thermal Conductivities in Crystalline Materials: Pure Silicon and Germanium. In *Length-Scale Dependent Phonon Interactions*, Shindé, S. L.; Srivastava, G. P., Eds. Springer New York: New York, NY, 2014; pp 115-136.
26. Srivastava, G. P., *The Physics of Phonons*. Taylor & Francis: 1990.
27. Casimir, H. B. G., Note on the conduction of heat in crystals. *Physica* **1938**, *5* (6), 495-500.
28. Mouhat, F.; Coudert, F.-X., Necessary and sufficient elastic stability conditions in various crystal systems. *Physical Review B* **2014**, *90* (22), 224104.
29. Meija, J.; Coplen, T. B.; Berglund, M.; Brand, W. A.; De Bièvre, P.; Gröning, M.; Holden, N. E.; Irrgeher, J.; Loss, R. D.; Walczyk, T.; Prohaska, T., Atomic weights of the elements 2013 (IUPAC Technical Report). *Pure and Applied Chemistry* **2016**, *88* (3), 265-291.
30. Ward, A.; Broido, D. A., Intrinsic phonon relaxation times from first-principles studies of the thermal conductivities of Si and Ge. *Physical Review B* **2010**, *81* (8), 085205.
31. Esfarjani, K.; Chen, G.; Stokes, H. T., Heat transport in silicon from first-principles calculations. *Physical Review B* **2011**, *84* (8), 085204.

Supplementary Information

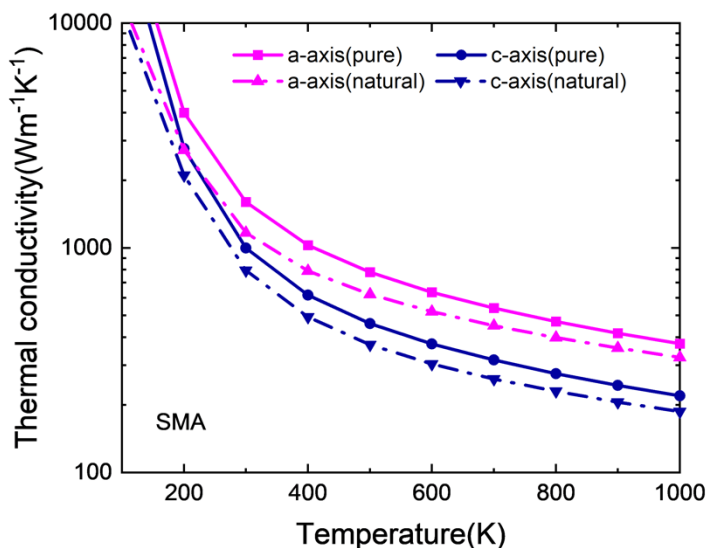


Figure S1: Temperature dependence lattice thermal conductivity of pure and naturally occurring h-BC₆N along a and c axis.